Local administration of IL-12 with an HC vector results in local and metastatic tumor control in pediatric osteosarcoma

Marta Zalacain,[1,2,3] María Bunuales,[1,4] Lucía Marrodan,[1,2,3] Sara Labiano,[1,2,3] Marisol Gonzalez-Huarriz,[1,2,3]
Naiara Martinez-Vélez,[1,2,3] Virginia Laspidea,[1,2,3] Montse Puigdelloses,[1,2] Marc García-Moure,[1,2,3]
Manuela Gonzalez-Aparicio,[1,4] Rubén Hernandez-Alcoceba,[1,4] Marta M. Alonso,[1,2,3,5] and Ana Patiño-García[1,2,3,5]

[1]Health Research Institute of Navarra (IDISNA), 31008 Pamplona, Navarra, Spain; [2]Program in Solid Tumors, Center for Applied Medical Research (CIMA), University of Navarra, 31008 Pamplona, Navarra, Spain; [3]Department of Pediatrics, Clínica Universidad de Navarra, 31008 Pamplona, Spain; [4]Program in Gene Therapy and Regulation of Gene Expression Program, Center for Applied Medical Research (CIMA), University of Navarra, 31008 Pamplona, Navarra, Spain

Osteosarcoma is the most frequent and aggressive bone tumor in children and adolescents, with a long-term survival rate of 30%. Interleukin-12 (IL-12) is a potent cytokine that bridges innate and adaptive immunity, triggers antiangiogenic responses, and achieves potent antitumor effects. In this work, we evaluated the antisarcoma effect of a high-capacity adenoviral vector encoding mouse IL-12. This vector harbored a mifepristone-inducible system for controlled expression of IL-12 (High-Capacity adenoviral vector enconding the EF1α promoter [HCA-EFZP]-IL-12). We found that local administration of the vector resulted in a reduction in the tumor burden, extended overall survival, and tumor eradication. Moreover, long-term survivors exhibited immunological memory when rechallenged with the same tumor cells. Treatment with HCA-EFZP-IL-12 also resulted in a significant decrease in lung metastasis. Immunohistochemical analyses showed profound remodeling of the osteosarcoma microenvironment with decreases in angiogenesis and macrophage and myeloid cell numbers. In summary, our data underscore the potential therapeutic value of IL-12 in the context of a drug-inducible system that allows controlled expression of this cytokine, which can trigger a potent antitumor immune response in primary and metastatic pediatric osteosarcoma.

INTRODUCTION

The American Cancer Society estimates that a total of 11,060 new pediatric cancer cases are diagnosed each year, with 1,190 deaths among children and adolescents in the United States.[1] Bone tumors represent 5% of all pediatric cancer cases, with osteosarcoma being the most aggressive. Osteosarcoma affects children and teenagers during their first or second decade of life, is associated with growth spurts, and is preferentially localized in large bones with high growth potential, such as the femur or tibia.[2] Even with the current multimodal treatment for osteosarcoma, which is based on pre- and postoperative polychemotherapy and surgery, the overall survival (OS) rate is approximately 70% and drops to less than 20% for those patients

who relapse or develop metastatic disease.[3,4] This poor survival underscores the urgent need for alternative effective therapeutic approaches. Interleukin-12 (IL-12) is a powerful cytokine, which due to its central role in bridging the innate and adaptive arms of immunity, has been extensively used as a therapeutic antitumor agent (reviewed in Colombo and Trinchieri[5]). IL-12 induces the activation of natural killer (NK) cells and T cells (both CD4+ and CD8+) and inhibits angiogenesis.[6] However, clinical trials in which IL-12 was administered systemically or subcutaneously showed severe toxicities, such as lethal inflammatory syndrome.[6–8] Therefore, several strategies, based on the use of a virus as a delivery system to allow local administration of IL-12, have been used.[9] One of these strategies involves the use of high-capacity adenoviral vectors (HC-AdVs), also known as helper-dependent or "gutless" vectors. These vectors are devoid of mostly all adenoviral sequences and therefore, harbor a large transgene coding space.[10] Based on this strategy, Wang et al.[11] developed an HC-AdV-encoding mouse IL-12 (mIL-12) with a mifepristone (Mif; RU)-inducible system for controlled liver-specific expression of IL-2 (HC-Ad/RUmIL-12). This approach allowed for high-level, liver-specific, and time-controlled IL-12 expression and resulted in a reduction in hepatic colon metastasis and an increase in the survival of these animals. Moreover, the combination of HC-Ad/RUmIL-12 with oxaliplatin further improved the therapeutic effect of the vector on hepatic colon cancer metastases.[12] The inducible system was further modified to eliminate all prokaryotic components and allow activity in all types of tumors, giving rise to the HCA-EFZP-IL-12 vector.[13] Based on these considerations, the focus of the present

Correspondence: Ana Patiño-García, Department of Pediatrics, Clínica Universidad de Navarra, 31008 Pamplona, Spain.
E-mail: apatigar@unav.es
Correspondence: Marta M. Alonso, PhD, Department of Pediatrics, Clínica Universidad de Navarra, 31008 Pamplona, Spain.
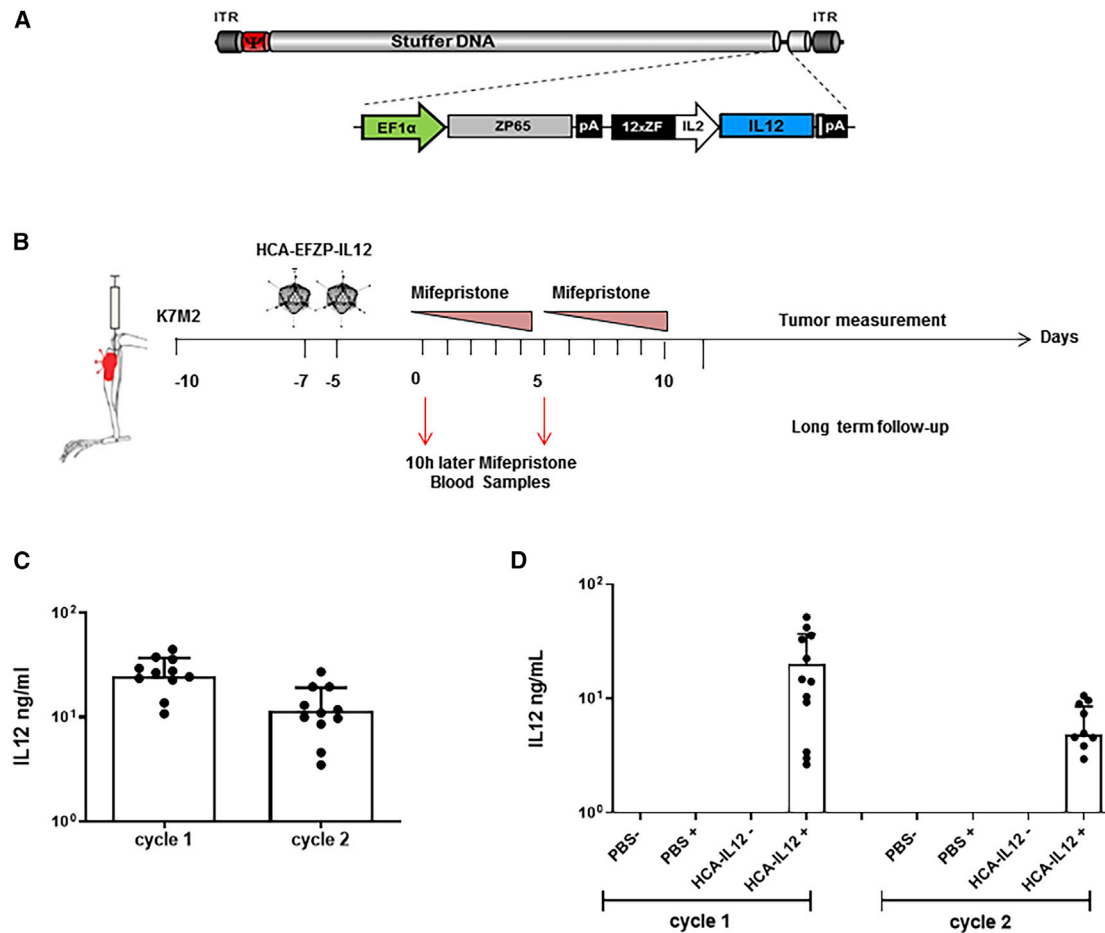**E-mail:** mmalonso@unav.es

Figure 1. The HCA-EFZP-IL-12 vector as a therapy for osteosarcoma

(A). Schematic illustration showing the backbone of the HC-AdV HCA-EFZP-IL-12. The adenovirus encodes mouse IL-12 (mIL-12) with a mifepristone (RU-486)-inducible system for controlled expression of IL-12. (B) Scheme of the experimental schedule. K7M2 murine osteosarcoma cells (5×10^5 per tibia) were injected into the tibial tuberosity of BALB/c mice (day −10). Animals were treated twice intratumorally with either a saline solution (control group) or 2×10^8 IU of HCA-EFZP-IL-12 (days −5 and −7). 3 days later, both groups were administered mifepristone intraperitoneally for 2 weeks with increasing doses (1 mg/kg on days 0–4, 4 mg/kg on days 7–9, and 8 mg/kg on days 10 and 11). Animals were sacrificed when they presented symptoms of disease, or the tumor volume reached 430 mm³. (C) Serum concentrations of IL-12 determined 10 h after mifepristone induction on the indicated days. (D) Determination of IL-12 specificity expression after mifepristone induction. K7M2 cells were engrafted into the tibial tuberosity following the same schedule as (B). Animals were randomized to four groups and serum concentration of IL-12 determined 10 h after mifepristone induction on the indicated days. The groups were as follows: (1) control without mifepristone (PBS−), (2) control plus mifepristone (PBS+), (3) HCA-EFZP-IL-12 without mifepristone (HCA-IL-12−), and (4) HCA-EFZP-IL-12 plus mifepristone (HCA-IL-12+).

work was to test the antitumor effect and safety of local administration of HCA-EFZP-IL-12 in a model of murine pediatric osteosarcoma.

RESULTS
Antitumor effect of HCA-EFZP-IL-12 on an immunocompetent osteosarcoma mouse model

The aim of this work was to evaluate whether intratumoral expression of IL-12 delivered with an HC-AdV and regulated by mifepristone would result in an antisarcoma effect (schematic representation of HCA-EFZP-IL-12; Figure 1A). To this end, osteosarcoma K7M2 cells were injected into the tibial tuberosity of immunocompetent mice,

followed by two intratibial injections of either PBS (control group) or HCA-EFZP-IL-12 (2×10^{11} infectious units [IUs]; treatment group) at 7 days after implantation (Figure 1B). Activation of the inducible system was carried out by intraperitoneal (i.p.) injection of mifepristone starting 3 days after the last vector injection. The induction regime consisted of two cycles of 5 consecutive days, as described in Materials and Methods. Tumor development and mouse weight were monitored twice per week until the end of the experiment (Figure 1B). To confirm the expression of IL-12, blood samples were collected 10 h after the first and sixth mifepristone injections. IL-12 was readily detected after induction cycle 1 and late induction (24.9 ± 12.2 and 11.63 ± 7.5 ng/mL, respectively; Figure 1C). To
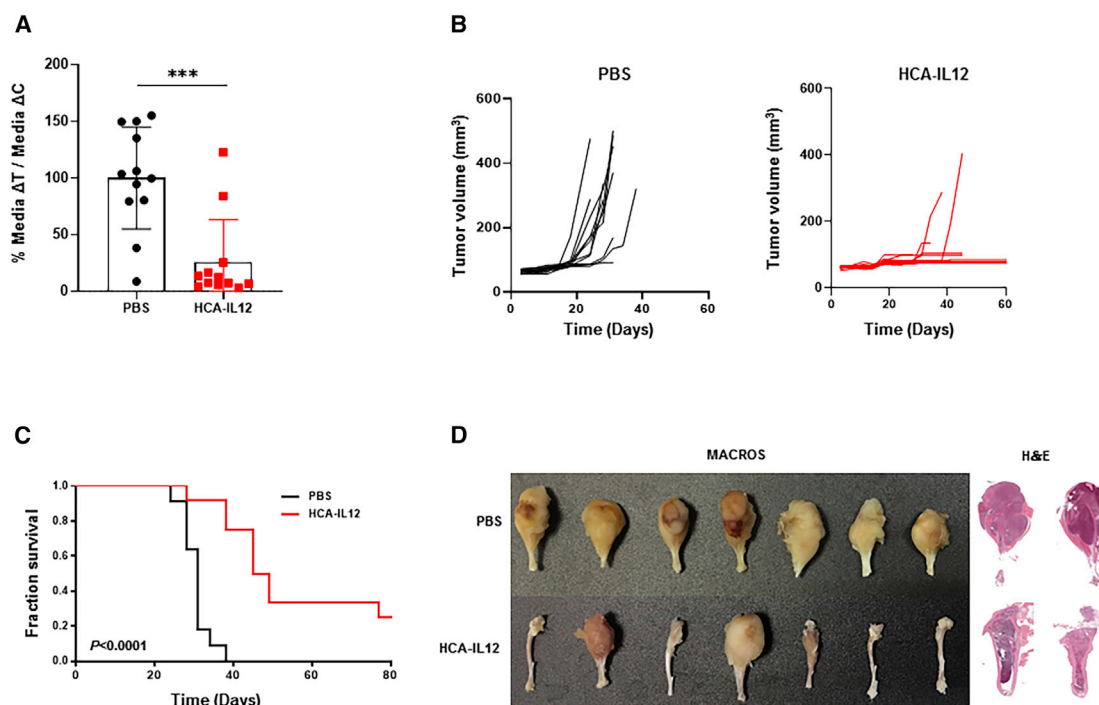
Figure 2. Characterization of the antisarcoma effect of the HCA-EFZP-IL-12 vector

Sarcoma-bearing mice were treated as described in Figure 1 and sacrificed on day 80. (A) Differences in tumor growth shown as percentages in comparison with the control groups. (B) Analyses of tumor burden development in the saline (control group) and HCA-EFZP-IL-12-treated (HCA-IL-12) groups. Tumor volume in the mouse tibias was measured on different days until the end of the experiment. (C) Survival curves. Graphs represent the overall survival of mice treated with HCA-EFZP-IL-12 (gray line) or PBS (black line). (D) Representative macroscopic images and H&E-stained sections of tibias from PBS- or HCA-EFZP-IL-12-treated mice.

confirm the specificity of the vector, we performed a second experiment that included the following groups: (1) PBS without mifepristone, (2) PBS plus mifepristone, (3) virus without mifepristone, and (4) virus with mifepristone. Again, blood samples were collected after the induction cycles. Importantly, we could only detect IL-12 expression in the group treated with the virus and mifepristone (20.2 ± 16.6 and 4.8 ± 3.3 ng/mL, cycle 1 and 2, respectively; Figure 1D). Tumor growth (DeltaT median/DeltaC median) was significantly bigger in the control group than in the HCA-EFZP-IL-12 group (100% ± 44.9% versus 25% ± 37.6%, respectively, p = 0.0002) (Figure 2A). All control mice developed visible bone tumors faster than the treated animals, and by day 20, all control mice showed measurable tumors (Figure 2B). Moreover, only 2 out of 12 tibias in the treated group developed tumors, which were not visible before day 35. The tumor diameters of the control mice ranged between 90 and 500 mm^3, whereas in the HCA-EFZP-IL-12-treated group, the only two tumors that grew presented volumes of 400 mm^3 and 288 mm^3 (Figure 2B).

Kaplan-Meier survival curves showed that local administration of HCA-EFZP-IL-12 led to significantly extended OS, with PBS-treated mice showing a median survival time of 31 days, whereas HCA-EFZP-IL-12-treated mice had a median survival time of 47 days (p < 0.0001; Figure 2C). Moreover, HCA-EFZP-IL-12 treatment of K7M2 cell-injected mice led to three long-term survivors (more than 80 days) (Figure 2C).

Macroscopically and pathologically, tumors had the characteristic morphology of osteosarcoma with notable production of malignant osteoid or immature bone (Figure 2D). In some control mice, the tumors had grown such that they crossed the epiphysis of the tibiae, penetrated the cortex of the bone, and destroyed it, resulting in transarticular tumors with some necrotic areas. In contrast, tibias from the treated mice looked normal macroscopically, and pathological analyses showed bones free of disease (Figure 2D). Finally, we assessed the expression of proliferation marker Ki67 and apoptosis marker caspase-3 by immunohistochemistry in tibias and lungs of both groups. We could not detect significant differences in either of these markers at the time point evaluated (sacrifice time; Figures S1A and S1B).

HCA-EFPZ-IL-12 vector treatment hinders the development of metastasis

To assess disease progression, we collected the lungs from the animals employed in the above experiment to quantify the extent of metastasis, a characteristic of osteosarcoma. In this experiment, 83.3% of the control mice showed metastasis (10/12), whereas only 58.3% (7/12) of HCA-EFZP-IL-12-treated mice showed tumors in the lungs (Figure 3A). Importantly, 2 out of the 7 mice that presented metastasis also presented a local tumor, as indicated above (Figure 2B); therefore, 42% of the mice were free of lung metastases. These data suggest that treatment with HCA-EFZP-IL-12 is able to control local
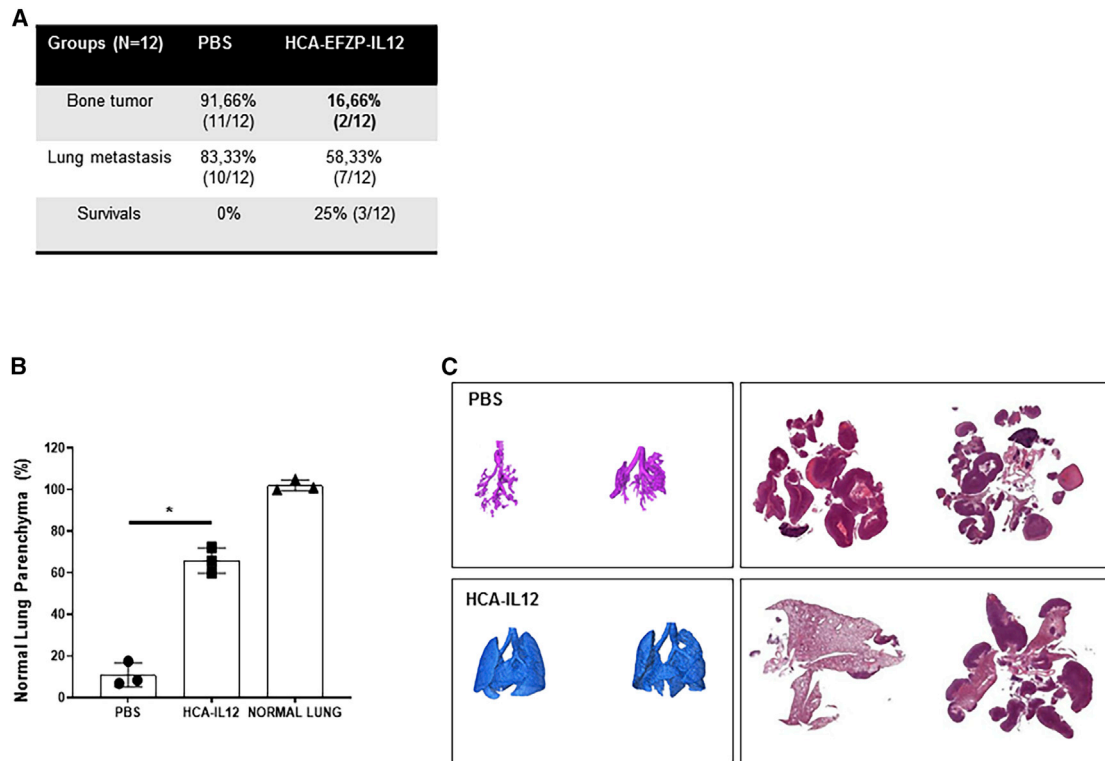
Figure 3. Administration of HCA-EFZP-IL-12 results in a significant decrease in the percentage of spontaneous lung metastasis

Sarcoma-bearing mice were treated as described in Figure 1 and sacrificed on day 80. (A) Table summarizing the percentages and raw numbers of primary tumor in the bone and spontaneous metastasis found in each group (PBS and HCA-EFZP-IL-12). (B and C) Evaluation of lung metastasis using micro-CT. Quantification of the normal lung parenchyma using micro-CT (B). Representative 3D image reconstruction of the normal lung parenchyma and corresponding histological macroscopic images of tumors in PBS- and HCA-EFZP-IL-12-treated animals (C).

disease; however, it is not so efficient at controlling the dissemination of lung metastases. In addition, we used micro-computed tomography (micro-CT) to detect lung metastases *in vivo* with high sensitivity. Micro-CT analysis showed that the integrity of the normal lung parenchyma was significantly preserved in mice treated with HCA-EFZP-IL-12 compared with control mice (p = 0.039; Figure 3B). Additionally, micro-CT imaging showed that treated mice harbored fewer tumor nodules than control mice (Figure 3C).

HCA-EFPZ-IL-12 vector treatment results in the development of partial immunological memory

To evaluate the generation of immunological memory, we reinjected K7M2 cells orthotopically in the three long-term survivors in the HCA-EFZP-IL-12-treated group. All of the control mice died within 25 days, with a median survival time of 23 days. In comparison, the HCA-EFZP-IL-12-treated mice had a median survival time of 63 days (p = 0.01; Figure 4A). Two out of the three treated (67%) mice showed protection against the rechallenge, indicating the development of immunological memory. Again, all of the control animals developed tumors earlier, with a median volume of 328.4 ± 136.8 mm^3 (Figure 4B). Pathological analyses of the rechallenged HCA-EFZP-IL-12-treated mice showed that one mouse was free of

disease (both in the bone and lungs) (Figure 4C). One of the other long-term survivors did not develop a primary bone tumor, but we found a lung metastasis. The third long-term survivor was sacrificed because of its tumor burden in the leg. These data suggest that treatment with HCA-EZP-IL-12 provides only partial protection against recurrent tumors.

Intratumoral injection of HCA-EFZP-IL-12 results in mild toxicity in a subset of mice

To assess the toxicity associated with the use of this powerful cytokine, we measured the body weight of mice, since body weight changes are one of the early indicators of toxicity. Our data showed a significant decrease in weight within the control group versus the HCA-EFZP-IL-12-treated group (19.4 gr versus 20.6 gr; p < 0.0001) (Figure S2A). In the virus-treated group, even though there was a slight reduction in body weight at the beginning of the experiment, most of the mice regained that weight by day 20. Additionally, we examined the liver of these mice, since IL-12 is known to induce hepatotoxicity.[14] We observed hepatic damage in 25% of the mice (3/12). Macroscopically, the affected livers presented a lighter appearance (Figure S2B). Nevertheless, none of the mice died from the hepatic alterations. Altogether, these data suggest that localized administration
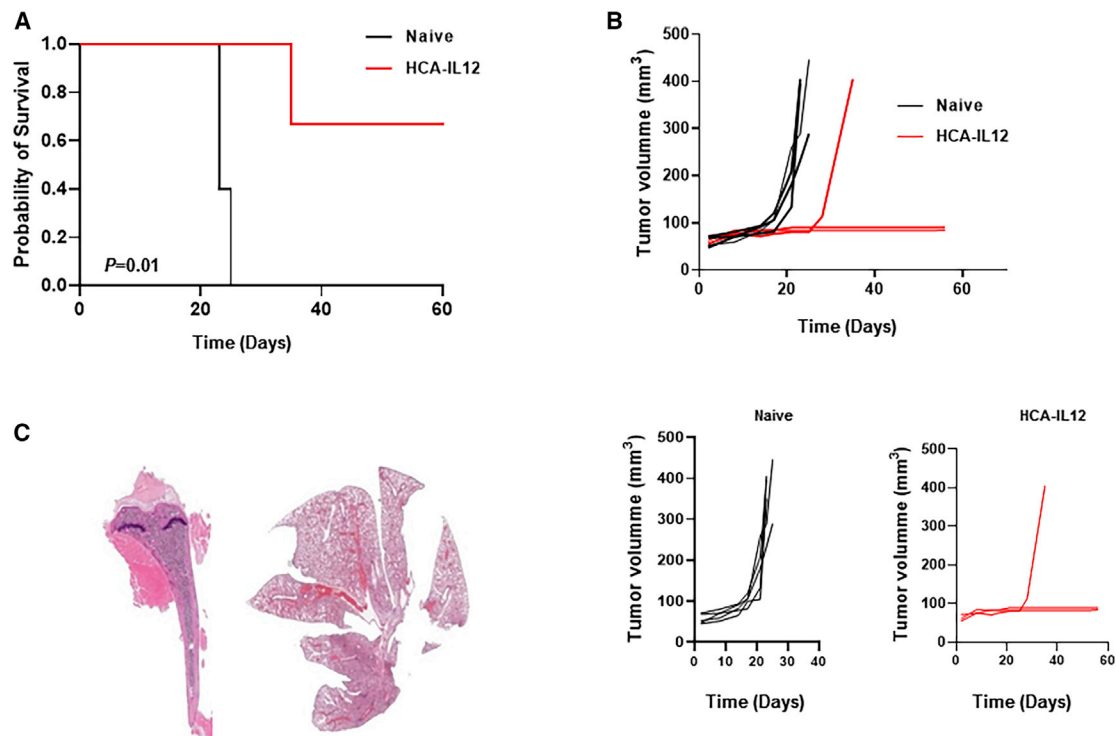
Figure 4. Treatment with the HCA-EFZP-IL-12 vector results in immunological memory in treated animals

(A) Rechallenge experiment performed with the long-term survivors identified in Figure 1D. The long-term survivors in the HCA-EFZP-IL-12-treated group (N = 3) were subjected to rechallenge with K7M2 cells and compared with PBS-treated control mice (N = 5). Kaplan-Meier survival curves were constructed, and the p value was calculated with the log-rank test (p = 0.0123). (B) Analyses of tumor burden development in the PBS group (control group) and HCA-EFZP-IL-12-treated group. Tumor volume in mouse tibias was measured on different days until the end of the experiment. (C) Representative macroscopic H&E images of the tibias and lungs from a long-term survivor. Note that the tissues are completely normal.

of IL-12 buffers the secondary side effects of IL-12 and that the displayed side effects were well tolerated.

HCA-EFZP-IL-12 treatment results in long-term remodeling of the local tumor and lung metastasis stroma

Since IL-12 is a very pleiotropic cytokine, we assessed its long-term effects on different cellular and stromal components. First, we analyzed T cell infiltration. Administration of HCA-EFZP-IL-12 increased CD3$^+$ cell infiltration compared to control treatment. However, the difference was not statistically significant (p = 0.21). Similarly, we observed an increase in CD8$^+$ cell infiltration (p = 0.07). We did not find any difference in FOXP3$^+$ cell infiltration between the groups (p = 0.63) (Figure S3A). We obtained similar results for lung metastasis (Figure S4A).

Since IL-12 is known to impair tumor angiogenesis, we next assessed the effect of local expression of this cytokine on this process. Interestingly, we observed a profound decrease in the expression of CD31 in the local tumor environment (p = 0.006) and spontaneous lung metastases (p < 0.0001) when we compared tumor tissue versus control tissue (Figure 5A). These data suggest that angiogenesis was disrupted, and this effect was maintained over time. We also observed

that intratumoral delivery of IL-12 had a striking effect on the macrophages, with these populations nearly disappearing from the primary tumor (p = 0.0047) and lung metastases (p < 0.0001) (Figure 5B). We obtained similar results when we assessed the myeloid (GR1$^+$) population. Although this cell population is much less abundant than the macrophage population in the osteosarcoma stroma, we observed a significant decrease in the population in the local tumor site in treated animals compared with PBS-treated animals (p < 0.0003; Figure 5C). We did not observe differences in this population in lung metastases (Figure 5C).

Altogether, these data suggest that IL-12 works at many levels, inducing remodeling of the tumor stroma that persists over time.

HCA-EFZP-IL-12 treatment results in T cell infiltration

To understand better the immune mechanism underlying the therapeutic effect of the HCA-EFZP-IL-12, we performed an additional *in vivo* study. This time mice were sacrificed 25 days after the induction of IL-12 with mifepristone, and the tumor-infiltrating lymphocytes (TILs) in bone and lung were characterized by flow cytometry (Figure 6A). We observed a significant increase in the CD4$^+$ and CD8$^+$ obtained from the tibias of the treated animals (Figure 6B).
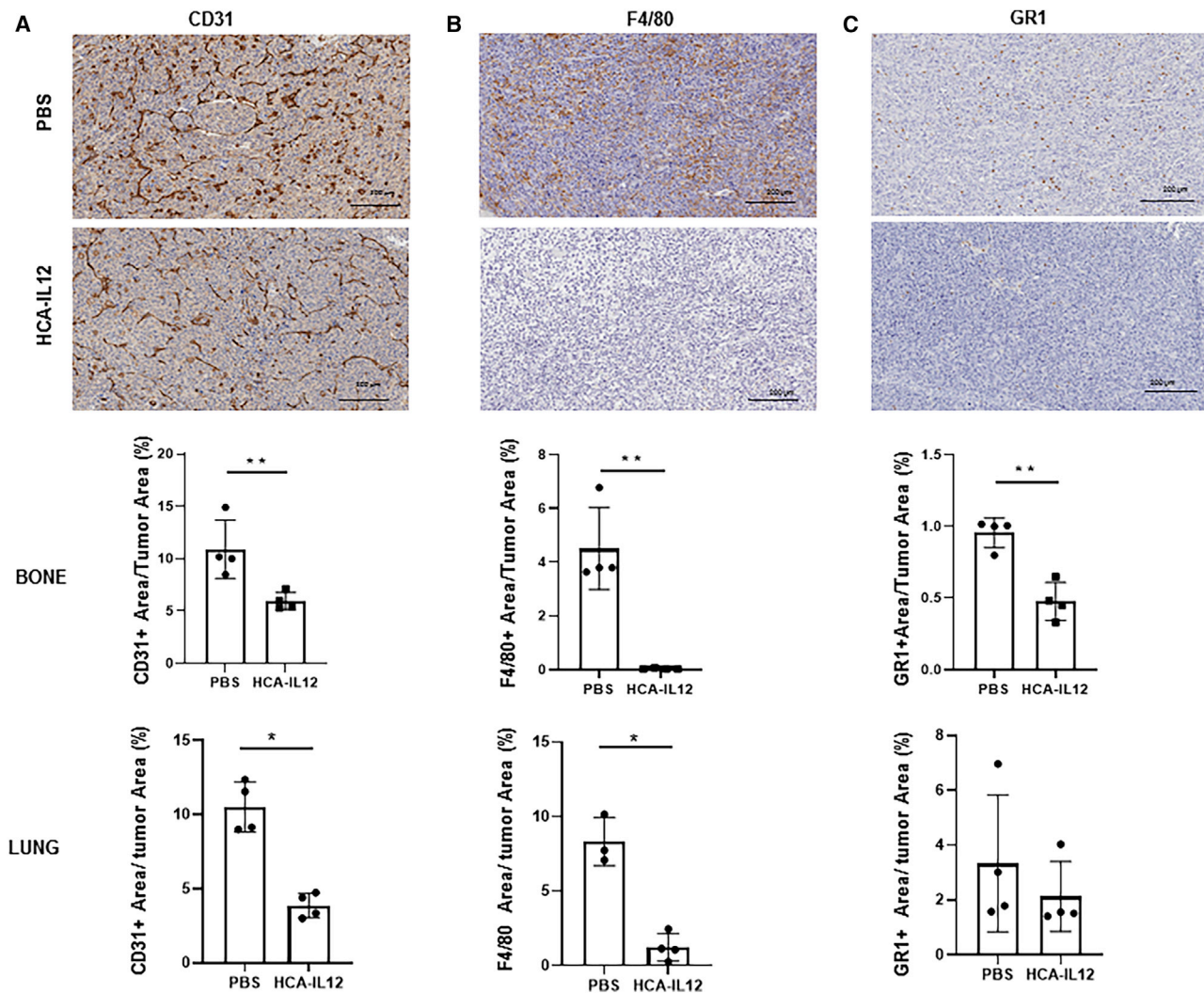
Figure 5. Local HCA-EFZP-IL-12 administration induces changes in the osteosarcoma microenvironment in the long term

(A−C) Sarcoma-bearing mice were treated as described in Figure 1 and sacrificed on day 80. Tumor samples were collected for analysis of CD31 (A), F4/80 (B), and GR1 (C). Upper panel: representative images (scale bar, 200 μm). Lower panels: quantification of the stained area as a percentage of the total area in bones and lungs (CD31, $p = 0.01$ and 0.02, respectively; F4/80, $p = 0.001$ and 0.05, respectively; and GR1, $p = 0.001$ and 0.2, respectively). Mann-Whitney test.

Similar results were obtained in the lungs of treated animals, where we observe an increase in NK cells and CD4$^+$ and CD8$^+$ cells (Figure 5C). We did not observe differences in either bone or lung in macrophages, dendritic cells, and regulatory T cells (Tregs; Figures 6B and 6C). These data suggest the triggering of an immune response following the induction of IL-12.

DISCUSSION

In this study, we demonstrated that HCA-EFZP-IL-12 administration caused a potent antitumoral effect on a murine model of pediatric osteosarcoma with spontaneous lung metastasis. We demonstrated that local administration of IL-12, using an HC-AdV, was able to control not only the local tumor but also lung metastasis development while maintaining a safe profile.

Although the antitumor effect of IL-12 has been extensively studied in numerous preclinical and clinical approaches (reviewed in Colombo and Trinchieri[5] and Del Vecchio et al.[6]), its therapeutic effect on osteosarcoma is not fully understood. Treatment with IL-12 upregulated Fas ligand expression in human osteosarcoma cells, and this mechanism is involved in the sensitivity of osteosarcoma cells to 4-hydroperoxycyclophosphamide.[15,16] In this line of thinking, intranasal delivery of IL-12 as an aerosol or with the aid of gene therapy improves the antisarcoma effect of ifosfamide in osteosarcoma lung metastasis.[17,18]

One of the caveats of IL-12 is that despite its potent antitumor effect, its clinical implementation has been hampered by its toxicity.[7,8,19] To overcome this hurdle, oncolytic viruses have been extensively utilized
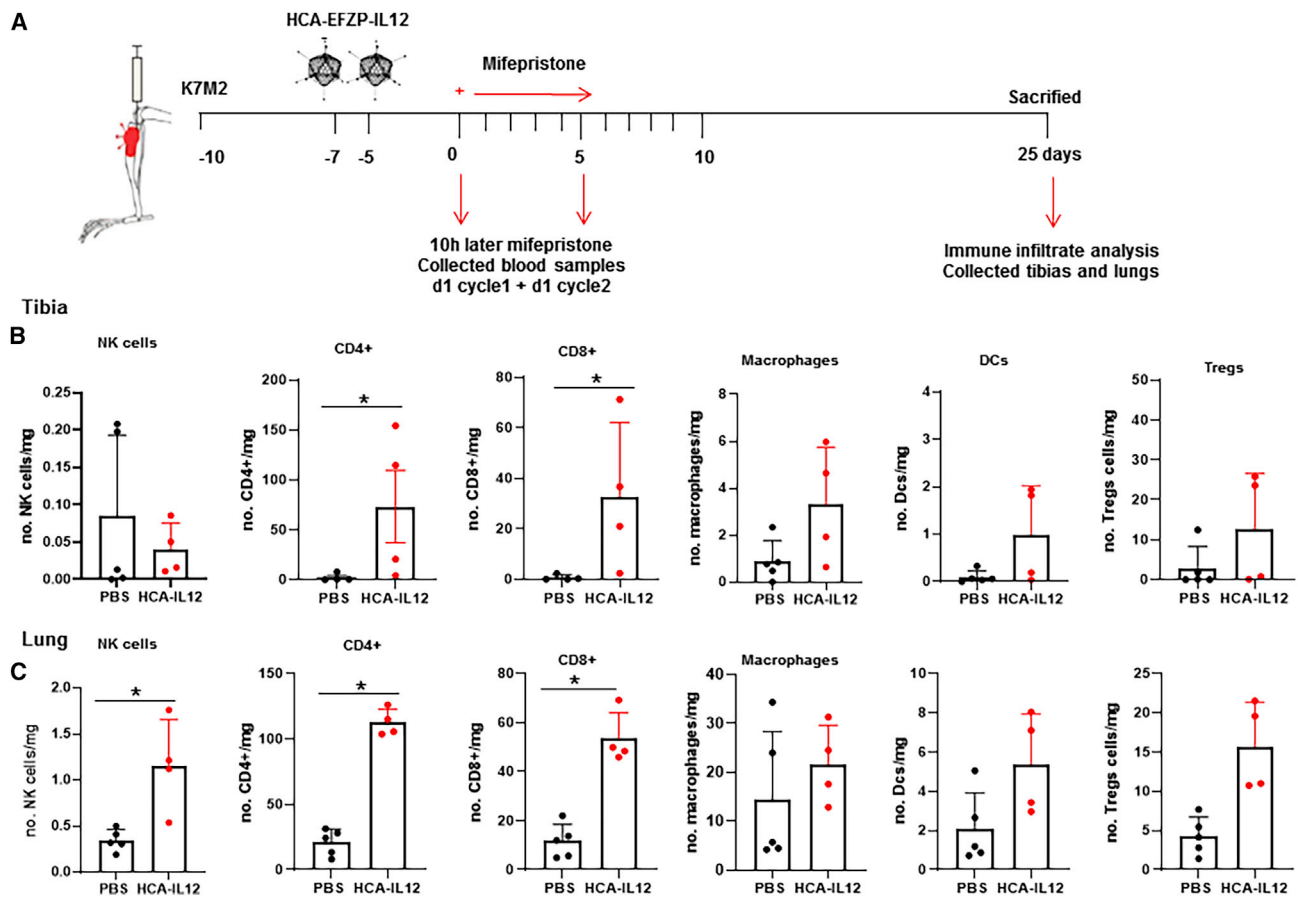
Figure 6. Local HCA-EFZP-IL-12 administration results in T cell infiltration in the osteosarcoma microenvironment

(A) Scheme of the experimental schedule. K7M2 murine osteosarcoma cells (5×10^5 per tibia) were injected into the tibial tuberosity of BALB/c mice (day −10). Animals were treated twice intratumorally with either a saline solution (control group) or 2×10^8 IU of HCA-EFZP-IL-12 (days −5 and −7). 3 days later, both groups were administered mifepristone intraperitoneally for 2 weeks with increasing doses (1 mg/kg on days 0–4, 4 mg/kg on days 7–9, and 8 mg/kg on days 10 and 11). Animals were sacrificed at day 25 after first mifepristone induction. (B and C) Flow cytometry of T cell populations in tumor-infiltrating lymphocytes (TILs) in tibia (B) or lung (C) of mice bearing K7M2 intratibial tumors at 25 days after IL-12 induction. Bars indicate mean ± SD (N = 4–5). Mann-Whitney test.

to deliver IL-2 intratumorally. For example, the herpes virus G47Delta-mIL-12 produced responses in glioblastoma models,[20,21] as have other viruses, such as adenovirus, Semliki Forest virus, and Newcastle disease virus (for a review, see Nguyen et al.[9]). One interesting strategy implemented to avoid systemic exposure to the cytokine consists of including IL-12 in the backbone of an adenovirus but deleting the N-terminal signal peptide to prevent IL-12 secretion. Delivered i.p., such an adenovirus was shown to produce a significant antitumor effect, which was reflected by enhanced survival and elimination of disseminated tumors on a pancreatic cancer model.[22] More importantly, treatment with this adenovirus showed no toxic effect when compared to treatment with an adenovirus carrying unmodified IL-12.

Other gene-therapy approaches have been used to deliver IL-12.[23] In this work, we used an HC-AdV to deliver the cytokine to tumors. Previously, a similar vector was very successful when used in combination with oxaliplatin to ameliorate the immunosuppressive microenvironment and eliminate metastases in a colorectal cancer model.[12] A replication-deficient (E1/E3-deleted) AdV carrying the IL-12 gene transcriptionally regulated by veledimex (an oral activator) has been assessed in a phase I clinical trial for recurrent high-grade gliomas (ClinicalTrials.gov: NCT02026271). In this trial, 31 patients were enrolled, and the data showed acceptable tolerability and evidence of an antitumor immune response.[24] Altogether, these works reflect the potential of delivering IL-12 to the tumor to limit the toxic effects of IL-12.

Currently, other systems utilizing adoptive cell therapy are being investigated. In this line of thinking, Etxeberria et al.,[25] using a very elegant approach, demonstrated that intratumoral delivery of IL-12 mRNA by transiently engineered antitumor CD8+ T cells resulted in a safe and effective immune response, epitope spreading, and control of distant metastasis. Again, this information indicates that there is a need to find strategies that circumvent the toxicity of this cytokine while taking full advantage of its therapeutic potential.

In this work, we employed an HC-AdV to deliver the cytokine to the tumor site in a controlled fashion. Compared with previous versions,[12] HCA-EFZP-IL-12 allows intratumoral administration and reduced leakage of transgene expression, increasing the safety of this approach.[13]

One of the attractive aspects of using IL-12 in this model was the profound effect of IL-12 on the tumor microenvironment. It is well known that the microenvironment determines tumor progression and metastasis. The presence and density of tumor-associated macrophages correlate with tumor cell proliferation, invasion, metastasis, and a poor prognosis.[26] We observed that macrophage numbers were greatly reduced after IL-12 treatment. M2 tumor-associated macrophages have been correlated with exhausted T lymphocytes in osteosarcoma and increased proinflammatory cytokine levels.[27] Moreover, these types of cells have also been described to be involved in tumor growth and vascularization.[28] Nevertheless, a limitation of our study was that although we did observe a decrease in macrophage numbers, we did not assess the functional status of this population. It would be interesting to elucidate whether in addition to the decrease, there is also a change in the functional status of the macrophages. We also observed that IL-12 treatment resulted in a significant decrease in the population of myeloid suppressor cells (GR1$^+$); the accumulation of this cell population in the osteosarcoma microenvironment is known to hamper the response to anti-PD-1 therapy.[29] Therefore, the combination of this vector with anti-PD-1 therapy could prove beneficial in osteosarcoma models.

We observed a striking effect of IL-12 treatment on the number of blood vessels (CD31). Whether this change was a direct effect of this cytokine on angiogenesis, a secondary effect due to the decrease in tumor-associated macrophage numbers, or both factors needs further elucidation. Of clinical significance, low vascular density in the tumor mass has been associated with a relatively good response to chemotherapy in a cohort of 131 osteosarcoma patients.[30] Based on this fact, one might speculate that IL-12 treatment could also sensitize patients to further chemotherapy treatment.

In summary, our results constitute proof-of-concept evidence for the potential of IL-12 as a therapeutic option for osteosarcoma. The understanding of the effect of this powerful cytokine can help us design more rational treatments for these rare tumors, which could be used in combination with immune checkpoint blockade agents to improve the survival and quality of life of all osteosarcoma patients.

MATERIALS AND METHODS
Cell line and culture conditions
The osteosarcoma cell line K7M2 (*ATCC CRL-836*) was purchased from the American Type Culture Collection (Sigma-Aldrich). The K7M2 cell line was derived by harvesting pulmonary metastases generated with the K7 murine osteosarcoma cell line, reimplanting the metastatic cells orthotopically, and repeating the harvest of a pulmonary metastasis lesion.[31] The cell line is considered highly aggressive with a reported pulmonary metastasis rate of over 90% in mice.

K7M2 cells were maintained in Dulbecco's modified Eagle's medium (DMEM), supplemented with 10% heat-inactivated fetal calf serum and 1% penicillin/streptomycin in an incubator at 37°C and 5% carbon dioxide. Cells were split when they reached approximately 70% to 80% confluence.

Viral vector
The HCA-EFZP-IL-12 vector has been previously described.[13] In this vector, all viral genes have been deleted and substituted with human noncoding DNA ("stuffer"), plus an expression cassette containing a ubiquitous mifepristone-inducible system for the expression of a single-chain version of mIL-12. The fully humanized ZP65 transactivator is controlled by the elongation factor 1α (EF1α) promoter. The vector was produced as previously described.[32] Purification was performed by double CsCl density gradient ultracentrifugation and desalting using Sephadex columns. Quantification of IU was performed by qPCR detection of vector genomes after a short infection of HEK293 cells, as described previously.[33] The titer was 1.77×10^{10} IU/mL with a total to infective particle ratio of 78.

Orthotopic intratibial murine model and treatment procedures
6- to 8-week-old female BALB/c mice were purchased from Charles River Laboratories (Wilmington, MA, USA). Animals were maintained under standard conditions, and all procedures were approved by the Institutional Ethical Committee (CEEA), in accordance with the guidelines of the University of Navarra. For orthotopic intratibial injection, the cortex of the tibial crest was penetrated using a 25-gauge needle. Cells were then injected with a second needle with a Hamilton syringe (500,000 cells/10 μL). 5 days after injection, the animals were randomized to receive either a saline solution (control) or 2×10^8 IU HCA-EZP-IL-12 (N = 12 per group). Treatment was administered by intratibial injection, and the vector was diluted in 10 μL of saline solution on days 5 and 7 after cell implantation.

Mifepristone (RU-486; Sigma, St. Louis, MO, USA) was dissolved in 100 μL of sesame oil and administered by i.p. injection, starting 10 days after cell implantation, which was defined as day 0 of treatment (Figure 1B). The induction regimen was designed to maintain IL-12 expression[12] and consisted of 2 cycles of 5 consecutive days. The doses were 1 mg/kg on days 0 to 4, 4 mg/kg on days 7–9, and 8 mg/kg on days 10 and 11. Both groups received mifepristone.

For the rechallenge experiment performed with the surviving mice, K7M2 (5×10^5 cells/mouse) cells were implanted in the previously implanted tibia and monitored until the end of the experiment.

Quantification of IL-12 levels
Blood samples were obtained by retro-orbital bleeding under inhaled anesthesia (isoflurane, Forane; Abbott Laboratories, Madrid, Spain), 10 h after mifepristone induction, and were collected the first day of each induction cycle. Serum was recovered by double centrifugation at 10,000 rpm for 5 min and stored at −20°C until use. The serum concentrations of mIL-12 (70 kDa) were determined with Opt E1A mIL-12 (p70) (BD Biosciences) enzyme-linked

immunosorbent assays. The quantification ranges for the IL-12 assay were 62.5–2,000 and 20–4,000 pg/mL, respectively. Dilutions ranging from 1:5 to 1:1,000 were used.

Primary bone tumor growth

Tumor sizes were determined by measuring 2 perpendicular diameters by using a caliper, and tumor volume was calculated by using the formula: volume = $D \times (d)^2 \times 0.5$, where D represents the largest diameter, and d represents the smaller diameter. Tumor volume was monitored serially using a digital caliper. Animals were sacrificed when the tumor volume of the tibia reached 430 mm^3 or when the corporal mass loss was more than 20%. The tibias, lungs, and liver were collected to perform different studies.

Immunohistochemical analysis

Organs were fixed for 24 h in 3.7%–4% w/v formaldehyde buffered to pH 7 and shaken at room temperature, followed by incubation for another 48 h in 70% ethanol. Tibias were decalcified in 4% ethylenediaminetetraacetic acid (EDTA) before embedding in paraffin.

Paraffin-embedded sections of mouse tibias and lungs were immunostained with antibodies specific to Ki67 (1:500; Cell Signaling Technology; 12202S), caspase-3 (1:500; Cell Signaling Technology; 9662), CD3 (1:150; Abcam; ab16669), CD8 (1:500; Cell Signaling Technology; 98941), Foxp3 (1:100; Cell Signaling Technology; 12653), CD31 (1:100; Cell Signaling Technology; 77699), GR1 (1:3,000; BioLegend; 108402), and F4/80 (1:200; Cell Signaling Technology; 70076), following conventional procedures and according to the manufacturers' instructions. Immunodetection was performed using biotinylated secondary antibodies and streptavidin horseradish peroxidase (HRP) complex (EnVision complex; Dako), and immune complexes were visualized with 3,3′-diaminobenzidine (DAB) substrate-chromogen (Dako, Glostrup, Denmark), followed by counterstaining with hematoxylin. Slides were scanned at 20× using Aperio CS2 (Leica Biosystem, Barcelona, Spain), regions of the samples were extracted using Aperio ImageScope version (v.)12.3.2.8013, and quantification was performed using Fiji/ImageJ platform 18.

In vivo pulmonary metastasis animal study

Thorax tomography scans were performed on mice anesthetized with an i.p. injection of ketamine and xylazine. Afterward, the mice were intratracheally cannulated and connected to a flexiVent rodent ventilator (Scireq, Montreal, QC, Canada) set at a rate of 200 breaths/min and a tidal volume of 10 mL/kg. Animals were kept breathing 2% isoflurane until completely relaxed.

Tomographic 3D images of the lungs were acquired using X-ray micro-CT (Quantum-GX; Perkin Elmer, Waltham, MA, USA) with the following parameters: 90 kVp X-ray source voltage, 88 μA current, and the high-speed scan protocol for a total acquisition time of 14 min and a gantry rotation of 360 degrees. Breathing-derived artifacts were de-noised using respiratory gating in each acquisition. Tomographic 3D images containing a whole lung had a total of 512 slices with an isotropic 72-μm voxel size and a resolution of 512 ×

512 pixels per slice. The analysis of lung volume in each sample was carried out using Fiji/ImageJ, an open-source Java-based image-processing software. Briefly, lung images were segmented by applying a fixed threshold, and total lung volume was measured over the obtained mask (cubic millimeters). Quantifications were normalized to the results for normal, healthy lung parenchyma.

Immune cell phenotyping

TILs were obtained from osteosarcoma and lung tumor samples and incubated for 15 min while rotating in 2 mL of DMEM plus 5 mg/mL collagenase (17-018-029; Roche) at 37°C. Next, DNase I (11-284-932-001; Roche) was added at final concentration of 10 μg/mL, and samples were mechanically excised and incubated for an additional 10 min at 37°C. Then, samples were mechanically disaggregated again and incubated for 10 min longer at 37°C. After the incubation, samples were filtered through a 40-μm cell strainer, and 10 mL of Hank's balanced salt solution (HBSS; 14175-053; Gibco) was added for centrifugation at $450 \times g$ (5 min at 4°C). The pellet was resuspended in 12 mL of HBSS containing 30% Percoll (17-0891-02; GE Healthcare) and 10% fetal bovine serum (FBS) and was centrifuged for 15 min at $800 \times g$ (4°C). Samples were rinsed with 10 mL of HBSS and centrifuged for 5 min at $450 \times g$ (4°C). Pellets were resuspended in 3 mL ammonium-chloride-potassium (ACK) buffer to remove erythrocytes. Finally, samples were centrifuged and resuspended in fluorescence-activated cell sorting (FACS) buffer for staining.

To identify the immune populations, immune infiltrates were surface stained with the following antibody panel: CD11c-PECy7 (BioLegend, San Diego, CA, USA), IA/IE-BV650 (BioLegend, San Diego, CA, USA), F4/80-allophycocyanin (APC; BioLegend, San Diego, CA, USA), NK1.1-BV605 (BioLegend, San Diego, CA, USA), CD11b-BUV395 (BioLegend, San Diego, CA, USA), and CD4-BUV496 (BioLegend, San Diego, CA, USA). Intracellular staining of Foxp3 using the mouse/human (mo/hu)Foxp3-PEeFluor610 antibody (eBioscience) was performed with the Foxp3/Transcription Factor Staining Buffer Set (eBioscience), according to the manufacturer's instructions. PromoFluor 840 maleimide (PromoKine) was used as a viability marker. Samples were acquired with the CytoFlex flow cytometer (Beckman Coulter), and data analyses were performed using FlowJo v.10 (FlowJo).

Statistical analysis

Data are expressed as the mean ± SD, and comparisons were performed using Mann-Whitney's t test. Statistical significance was defined as *$p < 0.05$, **$p < 0.01$, and ***$p < 0.001$. The survival of different treatment groups was compared using the log-rank test. The program GraphPad Prism 8 (Statistical Software for Sciences) was used for the statistical analyses.

SUPPLEMENTAL INFORMATION

Supplemental Information can be found online at https://doi.org/10.1016/j.omto.2020.11.003.

ACKNOWLEDGMENTS

AUTHOR CONTRIBUTIONS

Methodology, M.Z., M.B., M.G.-M., M.G.-H., V.L., S.L., M.P., and M.G.-A.; Writing − Original Draft, M.Z., M.M.A., and A.P.-G.; Funding Acquisition, M.Z., M.M.A., A.P.-G., and R.H.-A.; Review and Approval of the Manuscript, all authors.

DECLARATION OF INTERESTS

The authors declare no competing interests.

REFERENCES

1. Ward, E., DeSantis, C., Robbins, A., Kohler, B., and Jemal, A. (2014). Childhood and adolescent cancer statistics, 2014. CA Cancer J. Clin. 64, 83–103.

2. Bielack, S.S., Kempf-Bielack, B., Delling, G., Exner, G.U., Flege, S., Helmke, K., Kotz, R., Salzer-Kuntschik, M., Werner, M., Winkelmann, W., et al. (2002). Prognostic factors in high-grade osteosarcoma of the extremities or trunk: an analysis of 1,702 patients treated on neoadjuvant cooperative osteosarcoma study group protocols. J. Clin. Oncol. 20, 776–790.

3. Gorlick, R., and Khanna, C. (2010). Osteosarcoma. J. Bone Miner. Res. 25, 683–691.

4. Gorlick, R., Janeway, K., Lessnick, S., Randall, R.L., and Marina, N.; COG Bone Tumor Committee (2013). Children's Oncology Group's 2013 blueprint for research: bone tumors. Pediatr. Blood Cancer 60, 1009–1015.

5. Colombo, M.P., and Trinchieri, G. (2002). Interleukin-12 in anti-tumor immunity and immunotherapy. Cytokine Growth Factor Rev. 13, 155–168.

6. Del Vecchio, M., Bajetta, E., Canova, S., Lotze, M.T., Wesa, A., Parmiani, G., and Anichini, A. (2007). Interleukin-12: biological properties and clinical application. Clin. Cancer Res. 13, 4677–4685.

7. Motzer, R.J., Rakhit, A., Schwartz, L.H., Olencki, T., Malone, T.M., Sandstrom, K., Nadeau, R., Parmar, H., and Bukowski, R. (1998). Phase I trial of subcutaneous recombinant human interleukin-12 in patients with advanced renal cell carcinoma. Clin. Cancer Res. 4, 1183–1191.

8. Sangro, B., Mazzolini, G., Ruiz, J., Herraiz, M., Quiroga, J., Herrero, I., Benito, A., Larrache, J., Pueyo, J., Subtil, J.C., et al. (2004). Phase I trial of intratumoral injection of an adenovirus encoding interleukin-12 for advanced digestive tumors. J. Clin. Oncol. 22, 1389–1397.

9. Nguyen, H.-M., Guz-Montgomery, K., and Saha, D. (2020). Oncolytic Virus Encoding a Master Pro-Inflammatory Cytokine Interleukin 12 in Cancer Immunotherapy. Cells 9, 400.

10. Ricobaraza, A., Gonzalez-Aparicio, M., Mora-Jimenez, L., Lumbreras, S., and Hernandez-Alcoceba, R. (2020). High-capacity adenoviral vectors: Expanding the scope of gene therapy. Int. J. Mol. Sci. 21, E3643.

11. Wang, L., Hernández-Alcoceba, R., Shankar, V., Zabala, M., Kochanek, S., Sangro, B., Kramer, M.G., Prieto, J., and Qian, C. (2004). Prolonged and inducible transgene expression in the liver using gutless adenovirus: a potential therapy for liver cancer. Gastroenterology 126, 278–289.

12. Gonzalez-Aparicio, M., Alzuguren, P., Mauleon, I., Medina-Echeverz, J., Hervas-Stubbs, S., Mancheno, U., Berraondo, P., Crettaz, J., Gonzalez-Aseguinolaza, G., Prieto, J., and Hernandez-Alcoceba, R. (2011). Oxaliplatin in combination with liver-specific expression of interleukin 12 reduces the immunosuppressive microenvironment of tumours and eradicates metastatic colorectal cancer in mice. Gut 60, 341–349.

13. Poutou, J., Bunuales, M., Gonzalez-Aparicio, M., German, B., Zugasti, I., and Hernandez-Alcoceba, R. (2017). Adaptation of vectors and drug-inducible systems for controlled expression of transgenes in the tumor microenvironment. J. Control. Release 268, 247–258.

14. Poutou, J., Bunuales, M., Gonzalez-Aparicio, M., Garcia-Aragoncillo, E., Quetglas, J.I., Casado, R., Bravo-Perez, C., Alzuguren, P., and Hernandez-Alcoceba, R. (2015). Safety and antitumor effect of oncolytic and helper-dependent adenoviruses expressing interleukin-12 variants in a hamster pancreatic cancer model. Gene Ther. 22, 696–706.

15. Lafleur, E.A., Jia, S.F., Worth, L.L., Zhou, Z., Owen-Schaub, L.B., and Kleinerman, E.S. (2001). Interleukin (IL)-12 and IL-12 gene transfer up-regulate Fas expression in human osteosarcoma and breast cancer cells. Cancer Res. 61, 4066–4071.

16. Duan, X., Zhou, Z., Jia, S.F., Colvin, M., Lafleur, E.A., and Kleinerman, E.S. (2004). Interleukin-12 enhances the sensitivity of human osteosarcoma cells to 4-hydroperoxycyclophosphamide by a mechanism involving the Fas/Fas-ligand pathway. Clin. Cancer Res. 10, 777–783.

17. Duan, X., Jia, S.F., Koshkina, N., and Kleinerman, E.S. (2006). Intranasal interleukin-12 gene therapy enhanced the activity of ifosfamide against osteosarcoma lung metastases. Cancer 106, 1382–1388.

18. Jia, S.F., Worth, L.L., Densmore, C.L., Xu, B., Duan, X., and Kleinerman, E.S. (2003). Aerosol gene therapy with PEI: IL-12 eradicates osteosarcoma lung metastases. Clin. Cancer Res. 9, 3462–3468.

19. Cohen, J. (1995). IL-12 Deaths: Explanation and a Puzzle. Science 270, 908.

20. Cheema, T.A., Wakimoto, H., Fecci, P.E., Ning, J., Kuroda, T., Jeyaretna, D.S., Martuza, R.L., and Rabkin, S.D. (2013). Multifaceted oncolytic virus therapy for glioblastoma in an immunocompetent cancer stem cell model. Proc. Natl. Acad. Sci. USA 110, 12006–12011.

21. Saha, D., Martuza, R.L., and Rabkin, S.D. (2017). Macrophage Polarization Contributes to Glioblastoma Eradication by Combination Immunovirotherapy and Immune Checkpoint Blockade. Cancer Cell 32, 253–267.e5.

22. Wang, P., Li, X., Wang, J., Gao, D., Li, Y., Li, H., Chu, Y., Zhang, Z., Liu, H., Jiang, G., et al. (2017). Re-designing Interleukin-12 to enhance its safety and potential as an anti-tumor immunotherapeutic agent. Nat. Commun. 8, 1395.

23. Hernandez-Alcoceba, R., Poutou, J., Ballesteros-Briones, M.C., and Smerdou, C. (2016). Gene therapy approaches against cancer using in vivo and ex vivo gene transfer of interleukin-12. Immunotherapy 8, 179–198.

24. Chiocca, E.A., Yu, J.S., Lukas, R.V., Solomon, I.H., Ligon, K.L., Nakashima, H., Triggs, D.A., Reardon, D.A., Wen, P., Stopa, B.M., et al. (2019). Regulatable interleukin-12 gene therapy in patients with recurrent high-grade glioma: Results of a phase 1 trial. Sci. Transl. Med. 11, eaaw5680.

25. Etxeberria, I., Bolaños, E., Quetglas, J.I., Gros, A., Villanueva, A., Palomero, J., Sánchez-Paulete, A.R., Piulats, J.M., Matias-Guiu, X., Olivera, I., et al. (2019). Intratumor Adoptive Transfer of IL-12 mRNA Transiently Engineered Antitumor CD8+ T Cells. Cancer Cell 36, 613–629.e7.

26. Heymann, M.F., Lézot, F., and Heymann, D. (2019). The contribution of immune infiltrates and the local microenvironment in the pathogenesis of osteosarcoma. Cell. Immunol. 343, 103711.

27. Buddingh, E.P., Kuijjer, M.L., Duim, R.A.J., Bürger, H., Agelopoulos, K., Myklebost, O., Serra, M., Mertens, F., Hogendoorn, P.C., Lankester, A.C., and Cleton-Jansen, A.M. (2011). Tumor-infiltrating macrophages are associated with metastasis suppression in high-grade osteosarcoma: a rationale for treatment with macrophage activating agents. Clin. Cancer Res. 17, 2110–2119.

28. Li, X., Chen, Y., Liu, X., Zhang, J., He, X., Teng, G., and Yu, D. (2017). Tim3/Gal9 interactions between T cells and monocytes result in an immunosuppressive feedback loop that inhibits Th1 responses in osteosarcoma patients. Int. Immunopharmacol. 44, 153–159.

29. Jiang, K., Li, J., Zhang, J., Wang, L., Zhang, Q., Ge, J., Guo, Y., Wang, B., Huang, Y., Yang, T., et al. (2019). SDF-1/CXCR4 axis facilitates myeloid-derived suppressor cells accumulation in osteosarcoma microenvironment and blunts the response to anti-PD-1 therapy. Int. Immunopharmacol. *75*, 105818.

30. Kunz, P., Fellenberg, J., Moskovszky, L., Sápi, Z., Krenacs, T., Machado, I., Poeschl, J., Lehner, B., Szendrõi, M., Ruef, P., et al. (2015). Improved survival in osteosarcoma patients with atypical low vascularization. Ann. Surg. Oncol. *22*, 489–496.

31. Khanna, C., Prehn, J., Yeung, C., Caylor, J., Tsokos, M., and Helman, L. (2000). An orthotopic model of murine osteosarcoma with clonally related variants differing in pulmonary metastatic potential. Clin. Exp. Metastasis *18*, 261–271.

32. Gonzalez-Aparicio, M., Mauleon, I., Alzuguren, P., Bunuales, M., Gonzalez-Aseguinolaza, G., San Martín, C., Prieto, J., and Hernandez-Alcoceba, R. (2011). Self-inactivating helper virus for the production of high-capacity adenoviral vectors. Gene Ther. *18*, 1025–1033.

33. Jager, L., and Ehrhardt, A. (2009). Persistence of high-capacity adenoviral vectors as replication-defective monomeric genomes in vitro and in murine liver. Hum. Gene Ther. *20*, 883–896.